Accepted Manuscript

Development of an axially chiral $sp^3P/sp^3NH/sp^2N$-combined linear tridentate ligand—*fac*-Selective formation of Ru(II) complexes and application to ketone hydrogenation

Tomoya Yamamura, Satoshi Nakane, Yuko Nomura, Shinji Tanaka, Masato Kitamura

PII: S0040-4020(16)30070-9

DOI: 10.1016/j.tet.2016.02.007

Reference: TET 27477

To appear in: *Tetrahedron*

Received Date: 24 December 2015

Revised Date: 1 February 2016

Accepted Date: 2 February 2016

Please cite this article as: Yamamura T, Nakane S, Nomura Y, Tanaka S, Kitamura M, Development of an axially chiral $sp^3P/sp^3NH/sp^2N$-combined linear tridentate ligand—*fac*-Selective formation of Ru(II) complexes and application to ketone hydrogenation, *Tetrahedron* (2016), doi: 10.1016/j.tet.2016.02.007.

Graphical Abstract

To create your abstract, type over the instructions in the template box below.

Development of an axially chiral $sp^3P/sp^3NH/sp^2N$-combined linear tridentate ligand—*fac*-Selective formation of Ru(II) complexes and application to ketone hydrogenation

Leave this area blank for abstract info.

*Tomoya Yamamura, Satoshi Nakane, Yuko Nomura, Shinji Tanaka, and Masato Kitamura**
Graduate School of Pharmaceutical Sciences, Graduate School of Science, and Research Center for Materials Science, Nagoya University, Chikusa, Nagoya 464-8601, Japan

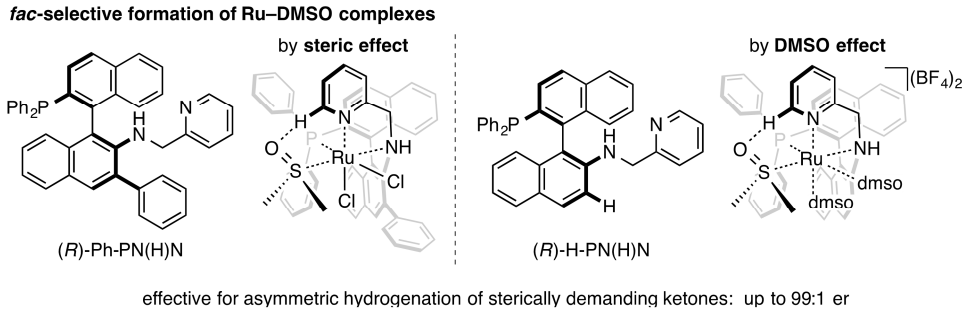

Fonts or abstract dimensions should not be changed or altered.

Tetrahedron
journal homepage: www.elsevier.com

Development of an axially chiral $sp^3P/sp^3NH/sp^2N$-combined linear tridentate ligand—*fac*-Selective formation of Ru(II) complexes and application to ketone hydrogenation

Tomoya Yamamura, Satoshi Nakane, Yuko Nomura, Shinji Tanaka, and Masato Kitamura*

Graduate School of Pharmaceutical Sciences, Graduate School of Science, Research Center for Materials Science, Nagoya University, Chikusa, Nagoya 464-8601, Japan

ARTICLE INFO

Article history:
Received
Received in revised form
Accepted
Available online

Keywords:
Chiral ligand
Tridentate
fac-Ru complex
Catalysis
Hydrogenation

ABSTRACT

A newly developed chiral linear tridentate ligand, R-PN(H)N (R = H or Ph), possesses Ph_2P and $PyCH_2NH$ groups at C(2) and C(2') positions of the 1,1'-binaphthyl skeleton without or with a C(3)-Ph substituent. The steric effect of C(3)-Ph and the electronic effect of the DMSO co-ligand realize the facial selective generation of *fac*-$RuCl_2$(Ph-PN(H)N)(dmso) and *fac*-[Ru(H-PN(H)N)(dmso)$_3$]$(BF_4)_2$, respectively. Both an H–Ru---sp^3N–H reaction site responsible for the donor–acceptor bifunctional catalyst (DACat) and a fence/plane chiral context were constructed by means of the following advantageous points: i) the sp^3P, sp^3N, and sp^2N ligating atoms have different electronic properties; ii) DMSO trans to sp^3N strongly coordinates to Ru and is fixed by a PyC(6)H---O=S hydrogen bond; and iii) the single NH function simplifies the DACat reaction site. The synergistic effect has led to success in the asymmetric hydrogenation of sterically demanding ketones. Structural characteristics of first-row transition metal complexes of R-PN(H)N have been also investigated.

1. Introduction

The steric and electronic properties of chiral ligands exert a significant effect on the performance of asymmetric molecular metal catalysis.[1] The chiral ligand should be appropriately designed and synthesized in accordance with properties of the central metal ion, including size, coordination number, and oxidation state change during a given reaction. The denticity, hapticity, hybridization of ligating atoms, and geometric isomerism should also be sufficiently considered so that the catalytic cycle turns over smoothly with efficient selection of the enantioface, enantioatom, or enantiomer of the substrate to give the chiral product with high enantiomer ratio (er). *

Most privileged chiral ligands[2] comprise C_2-symmetric bidentate organic molecules with the same ligating atoms, thereby theoretically reducing the number of reactive catalytic species. Increasing the types of ligating atom and denticity, as well as loss of symmetry, exponentially increases the number of ligand candidates, which raises the possibility of developing high-performance asymmetric catalysts. On the other hand, too many possibilities make the design concept difficult, provoking hesitation toward the development of unsymmetrical linear polydentate ligands even when the denticity is only three. An intrinsic disadvantage associated with linear tridentate ligands is the geometry isomerism that generates facial (*fac*) and meridional (*mer*) diastereomers in an octahedral metal complex

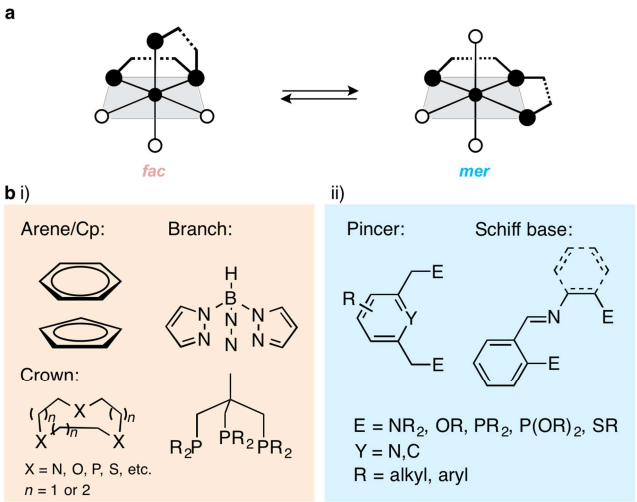

Fig. 1. (a) Geometry isomerism in an octahedral metal complex of a linear and flexible tridentate ligand and (b) general solutions to avoid the problem in the design of chiral tridentate ligands.

* Corresponding author. E-mail address: kitamura@os.rcms.nagoya-u.ac.jp (M. Kitamura).

(**Fig. 1a**). With tetrahedral, square planar, or trigonal bipyramidal complexes, the problem is not serious, as demonstrated in asymmetric reactions using Li, Zn, Cu, or Pd chemistry.[3] Although dependent on ligand structure, the higher thermodynamic stability of *mer* isomers as compared with *fac* isomers also tends to lessen, but not completely solve, the problem. There are mainly two types of positive approach to completely avoid such isomeric ambiguity, as shown in **Fig. 1b**: i) abandonment of the linear property; and ii) introduction of rigidity into the linear ligand skeleton. Geometrical restriction enables *fac*- or *mer*-selective formation of the octahedral metal complex. The former case i is exemplified by chirally substituted arene/Cp-type ligands,[4] scorpionate-type branched tripod ligands,[5] and crown-type macrocyclic tridentate ligands.[6] The latter case ii is represented by Pincer-type ligands possessing a benzene, pyrrole, or pyridine core with symmetrical or unsymmetrical side wingtips[7] and Schiff base-type ligands derived from salicylaldehyde, 2-formylpyridine, or a 1,3-diketone.[8]

A niche field remaining in the design of chiral tridentate ligands is the development of a linear and flexible ligand with all three different types of ligating atom in terms of element and/or hybridization.[9] Although the potential complications of *fac*/*mer* stereoisomers and λ/δ chelating conformations become obvious, the unsymmetrical situation together with non-identical ligating atoms has hidden potential for high-performance asymmetric molecular metal catalysis. A unique chirality may be constructed, and both the central metal and the coordination sites may be synergistically influenced. From this viewpoint, we have developed a new axially chiral $sp^3P/sp^3NH/sp^2N$-combined linear tridentate ligand, R-PN(H)N (**1**),[10] as shown in **Fig. 2**. In this article, we report details of the design concept, preparation, metal complex formation, and structural analyses, and its application to the asymmetric hydrogenation of ketones.

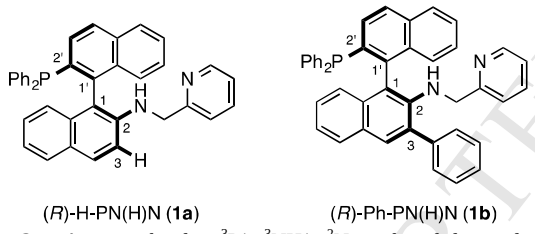

Fig. 2. A new chiral $sp^3P/sp^3NH/sp^2N$-combined linear ligand R-PN(H)N (**1**).

2. Results and discussion

2.1. Design concept

R-PN(H)N (**1**) was designed as an extension of the C_2-symmetric diphosphine BINAP.[11] The binaphthyl skeleton of BINAP in octahedral metal complexes is well known to construct a clear λ/δ seven-membered chelating conformation ((*R*)-BINAP: λ, (*S*)-BINAP: δ), and the pseudo-axial Ph substituent on the sp^3P atom is located nearly vertical to the sp^3P/sp^3P coordination plane to form a chiral fence.[12] Replacement of one of the PPh_2 groups of (*R*)-BINAP with a $PyCH_2NH$ moiety leads to (*R*)-H-PN(H)N ((*R*)-**1a**), in which the sp^3P atom adopts 3D spreading, while the sp^2N atom establishes a 2D planar region. Introduction of a Ph group at the C(3) position of the $PyCH_2NH$-substituted naphthalene ring gives (*R*)-Ph-PN(H)N ((*R*)-**1b**). These tridentate ligands can avoid both ligand dissociation and disproportionation to a 2:1 ligand/metal complex, a problem that bidentate ligands sometimes face. In both PN(H)N ligands, the sp^3NH function would endow a metal complex with intramolecular donor–acceptor bifunctional catalyst[13] (Intramol-DACat) ability (**Fig. 3a**) to realize, for example, the hydrogenation of ketones.[14–16] The single sp^3NH function in the R-PN(H)N ligand has the advantage of reducing the possible Intramol-DACat reactive sites in comparison to the corresponding multiple sp^3NH_2- and/or sp^3NH-containing systems.[17] Assuming an octahedrally configured *fac*- and *mer*-M(R-PN(H)N)L_3 complex (L is a neutral or anionic auxiliary ligand (co-ligand)), however, a complexity in the reaction site arises even with the single sp^3NH system. In the case that one L differs from the other two Ls, three different reaction sites are potentially generated both for the *fac* complex and for the *mer* complex. The total performance in terms of reactivity, selectivity, and productivity in a given asymmetric catalysis is averaged by the degree of contribution from these six isomers, which have their own performances.[18] Selective construction of the reaction site is a key issue for a high-performance catalyst. From this viewpoint, the three different ligating atoms in the R-PN(H)N ligand — soft sp^3P, hard and highly σ-donative sp^3N, and soft sp^2N — are expected to work to its advantage. In particular, the advantage is most obvious in the *fac* complex, in which all Ls locate trans to the sp^3P, sp^3N, and sp^2N atoms, exerting varying influence on the M–L bond strength according to the degree of σ-donicity and π-acceptor ability. The L that is trans to sp^3P is thought to be the most labile, being easily replaced by a nucleophile such as hydride and selectively generating a "H–M---N–H" Intramol-DACat reaction site (**Fig. 3a**, blue region). In this *fac* complex, unfortunately, no fence/plane-type chiral pocket can be constructed by the pseudo-axial Ph group on P and the $PyCH_2NH$ moiety, which are located above and below the sp^3P/sp^3N coordination plane, respectively. Moreover, as shown in **Fig. 3b**, the *fac* complex of (*R*)-**1a** is sterically less favored than the *mer* isomer: for an imaginary dicationic Ru(H-

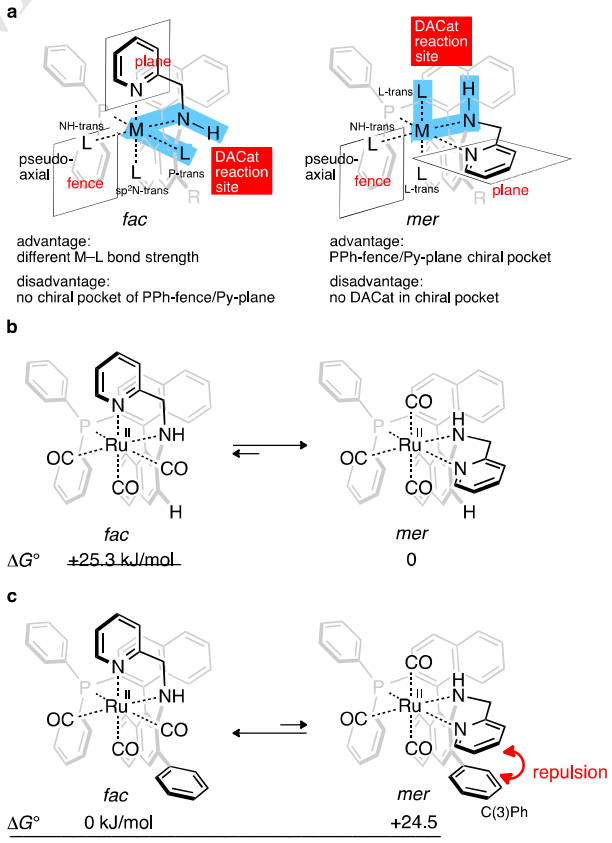

Fig. 3. (a) Characteristics of an octahedral metal complex of (*R*)-R-PN(H)N. (b) Stability difference between a dicationic *fac*-Ru((*R*)-H-PN(H)N)$(CO)_3$ and its *mer* isomer. (c) Stability difference between a dicationic *fac*-Ru((*R*)-Ph-PN(H)N)$(CO)_3$ and its mer isomer.

$PN(H)N)(CO)_3$ complex, in which the one-dimensional CO co-ligand has little steric effect, the *fac* complex is 25.3 kJ/mol less stable than the *mer* one. The energy profile is altered by the introduction of a Ph group at C(3) of (*R*)-**1a**, which stabilizes the corresponding *fac* complex of (*R*)-**1b** by 24.5 kJ/mol (**Fig. 3c**). Gauche-type steric repulsion (red arrow) between the C(3)Ph group and the $PyCH_2NH$ group in the *mer* isomer would shift the equilibrium to the *fac* side. Density functional calculations indicate that Ph-PN(H)N ((*R*)-**1b**) inherently forms the *fac* isomer with a octahedral-preferred central M, while H-PN(H)N ((*R*)-**1a**) requires an appropriate co-ligand L that would favor formation of the *fac* isomer. On the basis of these considerations, we decided to attempt the construction of the *fac* complex with an appropriate co-ligand L such as $(CH_3)_2S{=}O$ (DMSO). We hypothesized that the 3D spreading of DMSO might make a fence region instead of the PPh fence. For reference, the PPh-fence/Py-plane chiral pocket can be efficiently constructed in the *mer* isomer, but there is no DACat reaction site in the chiral pocket (**Fig. 3a**).

2.2. Ligand synthesis

The H-PN(H)N ligand was prepared, as shown in **Fig. 4a**, in 78% total yield (three steps and two pots) by i) the Staudinger-type reaction of (*R*)-**2a**[19] with 2-(azidomethyl)pyridine, ii) hydrolysis of the resulting iminophosphorane to the corresponding phosphine oxide, and iii) $PhSiH_3$ reduction of the phosphine oxide. The detailed procedure has been reported in the supporting information of the preceding short communication.[14b] In a similar way, (*R*)-Ph-PN(H)N was prepared in 80% yield from the triflate intermediate (*R*)-**2b**,[20] which was obtained in 87% yield by treatment of the corresponding known phosphine alcohol[21] with Tf_2NPh. Ligand (*R*)-**1b** was recrystallized from CH_3OH and CH_2Cl_2 (mp 188 °C). The molecular structure is shown in **Fig. 4b**. The absolute configuration was confirmed by Flack parameter analysis to be *R*.

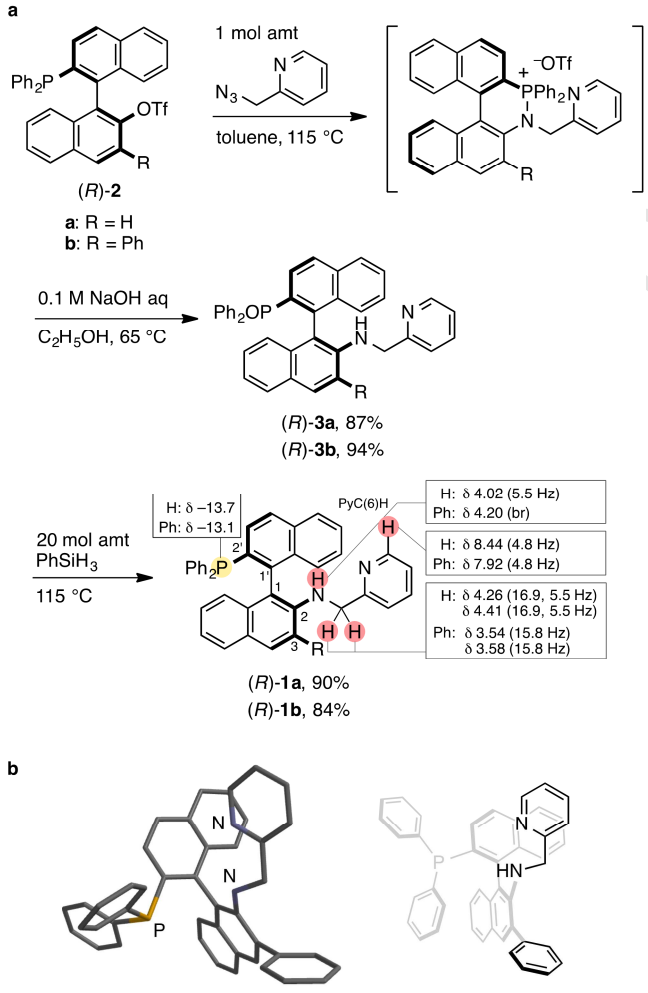

Fig. 4. (a) Preparation of (*R*)-H-PN(H)N ((*R*)-**1a**) and (*R*)-Ph-PN(H)N ((*R*)-**1b**). (b) Molecular structure of (*R*)-**1b** in crystal. P1 (#1), a = 9.088(4) Å, b = 10.730(5) Å, c = 17.001(7) Å, α = 87.249(13)°, β = 89.841(10)°, γ = 89.889(9)°, V = 1655.9(13) Å^3, Z = 2, R = 0.0590, R_w = 0.1278.

2.3. Metal complexes

2.3.1. Octahedral Ru(II) complexes

Complexes of Ru with an oxidation state of II are known to take a trigonal bipyramidal (TBP) or octahedral (OC) geometry,[22] depending on the property of the ligands. The geometry isomerism associated with the $sp^3P/sp^3NH/sp^2N$-combined ligand (*R*)-R-PN(H)N was investigated by using *fac*-$RuCl_2$(dmso-*S*)$_3$(dmso-*O*) (**4**)[23] as a stereochemically well-studied Ru precursor. The synthetic procedures, as well as the structural assignments, are summarized in **Fig. 5**.[20]xaaaaaaaaaaa

The reaction of (*R*)-H-PN(H)N ((*R*)-**1a**) with a 1 mol amount of **4** (THF, 120 °C, 30 min, microwave) quantitatively gave a ca. 3:2:1 stereoisomeric mixture of $RuCl_2$((*R*)-H-PN(H)N)(dmso) (**5**), the ^{31}P NMR signals of which appeared at δ 46.0, 41.1, and 34.5 in $CDCl_3$ (**Fig. 5a**). The major complex with the ^{31}P signal at δ 46.0 was separated as crystals, and X-ray crystallographic analysis determined the molecular structure as *mer*-$RuCl_2$((*R*)-H-PN(H)N)(dmso) (**5a**) with a DMSO-*S*/Cl trans arrangement (**Fig. 5b**). The seven-membered chelation made by sp^3P and sp^3N atoms to Ru takes a λ conformation with a dihedral angle of 77.7° for the binaphthyl skeleton. Consequently, the five-membered chelation of the $PyCH_SH_RNH$ moiety to Ru takes a δ conformation with the H_S–C–N–H and H_R–C–N–H dihedral angles of 167° and 49.0°, respectively. This geometric feature is reflected in the ^{1}H-NMR spectrum ($CDCl_3$), in which the three AMX-type H signals at δ 4.22 (J = 14.5 Hz (gem) and 2.1 Hz), δ 5.47 (J = 14.5 Hz (gem) and 11.6 Hz), and δ 7.06 (J = 11.6 Hz and 2.1 Hz) are assignable to H_R, H_S, and NH, respectively, on the basis of the Karplus equation. The second major complex (δ 41.1) was thought to be a DMSO-*S*/sp^3NH-trans *fac* isomer **5b** on the basis of the similarity of the NMR spectra (^{31}P δ 41.1; ^{1}H NMR δ 4.13 ($PyCH_SH_RNH$, J = 17.2 Hz (gem) and <3 Hz), 4.96 ($PyCH_SH_RNH$, J = 17.2 Hz (gem) and 10.3 Hz), 7.09 (NH, J: not assignable due to signal overlaps), δ 2.40 and 3.60 ($(CH_3)_2SO$)) to those of *fac*-$RuCl_2$((*R*)-Ph-PN(H)N)(dmso) (**6**) with a DMSO-*S*/sp^3NH trans arrangement (see **Fig. 5d**). The coordination of DMSO via its S or O atom is affected by the properties of the trans-located ligating atom and the metal ion.[24] In the present $RuCl_2$ complexes of the $sp^3P/sp^3NH/sp^2N$-combined ligand, DMSO coordinates to Ru through the S atom such that DMSO-*S* is trans to the ligating atom—either sp^3N or Cl—that has a high σ-donicity. The minor ^{31}P signal at δ 34.5 may be assigned to a DMSO-isomeric *mer* complex **5c** on the basis of the ^{1}H-NMR similarity to that of **5b** (**Fig. 5d**).aaaaaaaaaaaaaaaaaaaaaaaaaaaaa

Under the same conditions as those for (*R*)-**1a**, the C(3)-Ph-substituted (*R*)-Ph-PN(H)N ligand ((*R*)-**1b**) was allowed to react with **4** to give a single stereoisomer quantitatively, as estimated from the ^{31}P-NMR analysis (**Fig. 5c**). Single crystals were obtained in 53% yield from CH_3OH, and the molecular structure was determined by X-ray crystallographic analysis as *fac*-$RuCl_2$((*R*)-Ph-PN(H)N)(dmso) (**6**) with a DMSO-*S*/sp^3N trans arrangement (**Fig. 5d**). The sp^3P and sp^3N atoms coordinate to Ru to generate a λ conformation with a dihedral angle of 71.8° (binaphthyl skeleton), and the $PyCH_SH_RNH$ moiety connecting to C(2) is flipped up to the Ph_2P-connected naphthalene side. The *fac* coordination of the Ph-PN(H)N ligand results in the

geometrical arrangement of $PyCH_SH_RNH$ with H_S–C–N–H and H_R–C–N–H dihedral angles of 108.5° and 9.2°, respectively, and with the H_S atom in close proximity to the C(8')H of the naphthalene ring (2.685 Å). The remaining three coordination sites are occupied by DMSO and two chloride anions, which are located trans to sp^3N, sp^3P, and sp^2N, respectively. The highly electron donative sp^3N atom, which has no ability to accept Ru-d orbital back donation, enhances the orbital interaction between the Ru-d orbital and the σ^*_{S-O} of DMSO. The synergistic effect of the electrostatic and orbital factors shortens the Ru–S bond length to 2.265 Å from the length observed in a trans sp^3P---Ru---S=O system (2.30–2.35 Å).[25] The existence of a hydrogen bond between the sulfur-bound DMSO oxygen atom and PyC(6)H is suggested by the short distance, 2.639 Å, and the small sp^2N---Ru---S=O dihedral angle, 6.6°. The PyC(6)H---O=S interaction further stabilizes the complex, and determines the conformation of the DMSO co-ligand such that one of the CH_3 groups is sticking out toward the sp^3P/sp^3N in-plane coordination site and the other CH_3 group is located obliquely above the pseudo-equatorial phenyl substituent on the sp^3P atom. The molecular structure observed in the crystal was fully consistent with the ^{1}H-NMR behavior in $CDCl_3$ (**Fig. 5d)**. The three H signals in the $PyCH_SH_RNH$ moiety show an AMX pattern at δ 4.14 (H_S, J = 17.2 Hz (gem) and 2.1 Hz), δ 4.98 (H_R, J = 17.2 Hz (gem) and 10.3 Hz), and δ 7.92 (NH, J = 10.3 Hz and <3 Hz), and the H_S proton has a cross signal with the naphthalene C(8')H in the ROESY spectrum (2.4% nOe).[20] The two diastereotopic CH_3 groups of DMSO resonate at δ 2.22 and 3.38. The 1.2-ppm downfield shift can be ascribed to the fact that the CH_3 group is located in the deshielding region of the pseudo equatorial Ph substituent on the sp^3P atom. Consistent with the existence of a PyC(6)H---O=S hydrogen bond, the PyC(6)H signal appears at δ 9.92, which is 2 ppm lower as compared with the ligand itself (δ 7.92; see **Fig. 4a**).[26] aaaaa aaaaa aaaaa aaaaa aaaaa

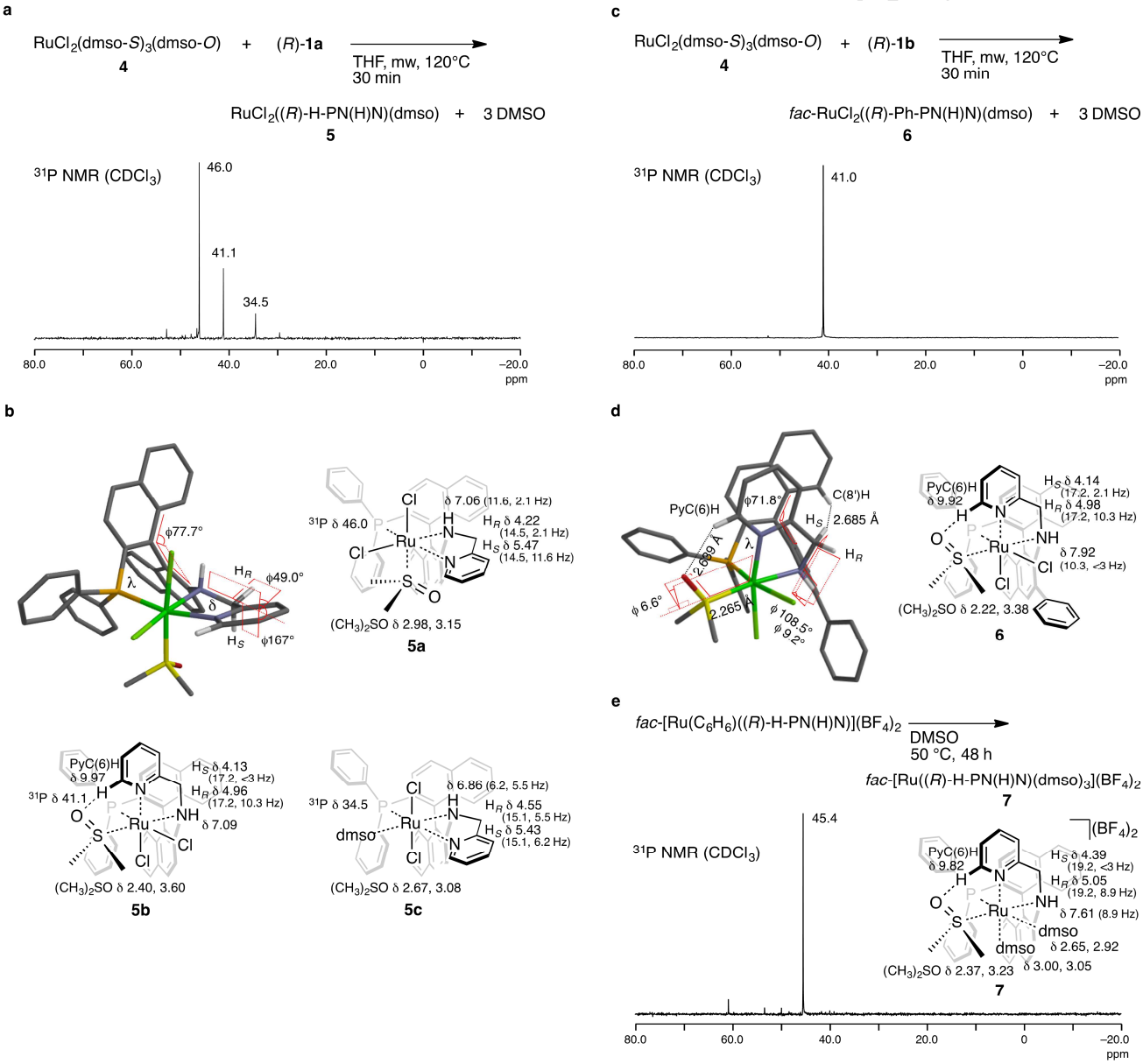

Fig. 5. Preparation of octahedral R-PN(H)N–Ru complexes and the structural analyses. Typical ^{1}H-NMR signals in $CDCl_3$ are shown on the chemical structures. (a) Ru–DMSO complex formation of $RuCl_2$(dmso-*S*)$_3$(dmso-*O*) (**4**) and (*R*)-H-PN(H)N ((*R*)-**1a**) and the ^{31}P-NMR spectrum. (b) Molecular structure of *mer*-$RuCl_2$((*R*)-Ph-PN(H)N)(dmso) (**5a**) (δ 46.0) in crystal. $P2_1$ (#4), a = 11.538(7) Å, b = 11.624(7) Å, c = 13.723(9) Å, β = 97.471(8)°, V = 1825(2) Å^3, Z = 2, R = 0.0856, R_w = 0.2564. The supposed structures of the second major complex **5b** (δ 41.1) and the minor complex **5c** (δ 34.5) are shown. (c) Preparation of *fac*-$RuCl_2$((*R*)-Ph-PN(H)N)(dmso) (**6**) from **4** and (*R*)-Ph-PN(H)N ((*R*)-**1b**) and the ^{31}P-NMR spectrum. (d) Molecular structure of **6** in crystal. $P2_12_12_1$ (#19), a = 12.359(4) Å, b = 16.791(5) Å, c = 18.602(5) Å, V = 3860(2) Å^3, Z = 4, R = 0.0912, R_w = 0.2428. (e) Preparation of *fac*-[Ru((*R*)-H-PN(H)N)(dmso)$_3$](BF$_4$)$_2$ (**7**) from *fac*-[Ru(C$_6$H$_6$)((*R*)-H-PN(H)N)](BF$_4$)$_2$[27] and the ^{31}P-NMR spectrum.

fac-Selective generation of the Ru complex even with the C(3)-non-substituted (*R*)-H-PN(H)N ((*R*)-**1a**) was attained on the basis that the trans arrangement of two DMSOs on Ru, O=S---Ru---S=O, is energetically disfavored.[24] Thus, treatment of *fac*-[Ru(C_6H_6)((*R*)-H-PN(H)N)](BF_4)$_2$ with DMSO at 50 °C for 48 h followed by evaporation gave *fac*-[Ru((*R*)-H-PN(H)N)(dmso)$_3$](BF_4)$_2$ (**7**) (**Fig. 5e**).[27] In view of the NMR behavior of the above two Ru complexes, NMR analysis in $CDCl_3$ supported a structure in which the facial stereochemistry was retained after replacement of the benzene ligand with three DMSOs. The DMSO ligands showed three sets of signals for the two methyl H atoms at δ 2.37 and δ 3.23, δ 3.00 and δ 3.05, and δ 2.65 and δ 2.92; these sets were assigned by cross signal analysis of the H-H COSY spectrum.[27] Furthermore, the DMSO that was trans to sp^{3}N was found to be stabilized by a six-membered hydrogen bond between the DMSO oxygen atom and C(6)H of the Py moiety in the ligand, as supported by the low C(6)H chemical shift (δ 9.82) similar to that of **6** (δ 9.92). The ^{1}H-NMR behavior of PyCH$_S$H$_R$ and NH (δ 4.39 (H$_S$, *J* = 19.2 Hz (gem) and <3 Hz), 5.05 (H$_R$, *J* = 19.2 Hz (gem) and 8.9 Hz), and 7.61 (NH)) was also consistent with the *fac*-determined Ru complex **6**.

2.3.2. Non-octahedral metal complexes

For reference, **Fig. 6** shows the molecular structures of first-row transition metal complexes of the R-PN(H)N ligands (*R*)-**1a** and (*R*)-**1b**. All of the structures of the Cu(I), Fe(II), Co(II), and Ni(II) complexes were determined by X-ray crystallographic analyses of single crystals.[20] The selected structural parameters are also summarized in **Fig. 6**. The coordination geometry varied from uncommon trigonal monopyramidal (TMP) to square monopyramidal (SMP) or trigonal bipyramidal (TBP),[22] depending on the central metal ion and the presence or absence of a C(3) substituent. The four- and five-coordinate geometries were analyzed by using the conventional τ_4 and τ_5 indexes, respectively: τ_4 = [Σ(basal–M–basal) – Σ(basal–M–axial)]/90° (τ_4 = 0 (tetrahedral (Td)); τ_4 = 1 (TMP)). τ_5 = (α – β)/60° (α, β = basal angles; τ_5 = 0 (SMP); τ_5 = 1 (TBP)).[28]xxxxxxxxxxxxxxxx

CuCl((*R*)-H-PN(H)N) was prepared from CuCl and (*R*)-**1a** in a 1:1 ratio (10 mM each, THF, reflux, 18 h). Recrystallization from a 1:3 $CHCl_3$–Et_2O mixture afforded yellow chunky crystals (ca. 30% yield). As shown in **Fig. 6a**, the Cu(I) complex takes a TMP geometry with sp^{3}P, sp^{2}N, and Cl in the basal plane (thin red lines) and sp^{3}N at the apex. The sum of the angles in the trigonal plane is 359.7° (sp^{2}N–Cu–sp^{3}P = 132.7°, sp^{2}N–Cu–Cl = 99.6°, and sp^{3}P–Cu–Cl = 127.4°), and the average angle of the axial sp^{3}N from the trigonal plane is 91.1° (sp^{3}N–Cu–sp^{3}P = 99.2°, sp^{3}N–Cu–sp^{2}N = 78.7°, and sp^{3}N–Cu–Cl = 95.45°). The τ_4 value is calculated to be 0.96, clearly indicating ideal TMP geometry. The sp^{3}N–Cu bond length of 2.403 Å is longer than usual. The sp^{3}N is thought to weakly coordinate to Cu in the basal trigonal plane. TMP complexes are not common, and are generally prepared by using specially designed ligands, including tripodal tetradentate ligands[29] and PNN-pincer-type iminophosphorane ligands,[30] in combination with Fe(II), Co(II), Ni(II), Zn(II), and Cu(I). The sp^{3}P/sp^{3}NH/sp^{2}N-combined (*R*)-H-PN(H)N ligand may have certain steric and electronic characteristics that facilitate generation of a Cu(I) complex with TMP geometry. Such a TMP Cu(I) complex with a τ_4 value of near 1 is the first example of its kind.[31]xxxxxxxxxxxxxxxxxxxxxxxx

With Fe(II), Co(II), and Ni(II) ions, (*R*)-R-PN(H)N ((*R*)-**1**) formed a 1:1 complex with SMP or TBP geometry. FeX$_2$((*R*)-R-PN(H)N) (X = Cl or Br; R = H or Ph) was prepared by mixing Fe(II)X$_2$ with (*R*)-**1** in a 1:1 ratio in CH_3CN (60 mM each; 100 °C; 12 h). Cooling down to rt afforded single crystals in 30%–60% yields (FeCl$_2$((*R*)-H-PN(H)N), yellow prism; FeBr$_2$((*R*)-H-PN(H)N), yellow blocks; FeCl$_2$((*R*)-Ph-PN(H)N), yellow prism; FeBr$_2$((*R*)-Ph-PN(H)N), green chunks). The coordination geometry of FeCl$_2$((*R*)-H-PN(H)N) was close to SMP (**Fig. 6b**), in which the sp^{3}P, sp^{3}N, sp^{2}N, and Cl ligating atoms occupy the basal plane and another Cl is located at the apex. The sum of the angles in the basal plane is 348.8° (sp^{2}N–Fe–sp^{3}N = 75.3°, sp^{3}N–Fe–sp^{3}P = 84.15°, sp^{3}P–Fe–Cl(basal) = 95.45°, and Cl(basal)–Fe–sp^{2}N = 93.85°), and the average angle of the axial Cl from the square plane is 102.3° (sp^{2}N–Fe–Cl(apical) = 109.1°, sp^{3}N–Fe–Cl(apical) = 95.85°, sp^{3}P–Fe–Cl(apical) = 95.2°, and Cl(basal)–Fe–Cl(apical) = 109.15). The difference of the two angles made by two atoms at the opposite corners of the basal plane is only 5.5° (τ_5 = 0.09) (sp^{2}N–Fe–sp^{3}P = 149.4° and sp^{3}N–Fe–Cl(basal) = 154.9°), showing that the geometry is closer to SMP than to TBP. Replacement of Cl with Br had little effect on the SMP geometry (sp^{2}N–Fe–sp^{3}P = 149.2° and sp^{3}N–Fe–Br(basal) = 157.7°; τ_5 = 0.14) except for the bond lengths (**Fig. 6c**). In FeBr$_2$((*R*)-H-PN(H)N), the bond lengths of sp^{3}P–Fe and sp^{2}N–Fe are 0.02 and 0.01 Å longer, respectively. One CH_3CN molecule per Fe(II) ion was present in the crystals,[20] but an octahedral geometry involving CH_3CN was not formed. Reaction of FeBr$_2$((*R*)-H-PN(H)N) with CO (1 atm, $CDCl_3$, rt, 1 h) resulted in no change. Introduction of a C(3)Ph substituent in the naphthalene ring changed the coordination geometry to the TBP side (τ_5 = 0.43 (Cl; sp^{2}N–Fe–sp^{3}P = 162.9° and sp^{3}N–Fe–Cl(basal) = 136.4°) and τ_5 = 0.42 (Br; sp^{2}N–Fe–sp^{3}P = 163.3° and sp^{3}N–Fe–Br(basal) = 138.3°)) (**Fig. 6d–e**). In comparison to the H-PN(H)N case, the sp^{3}N–Fe–Cl(basal) angle (136.4°) was narrowed by 18.5°, while the sp^{2}N–Fe–sp^{3}P angle (162.9°) was widened by 13.5°. The same tendency was observed for the FeBr$_2$ complex. Steric repulsion between the C(3)Ph group and the PyCH$_2$NH group would alter the sp^{2}N–Fe bond, changing the SMP geometry to TBP-like one.

Reaction of $CoCl_2$ with (*R*)-**1a** in a 1:1 ratio (10 mM each, THF, rt, 18 h), followed by concentration and recrystallization from a 1:3 THF–Et_2O mixture gave single crystals of CoCl$_2$((*R*)-H-PN(H)N) (ca. 30% yield; blue prism). NiCl$_2$((*R*)-H-PN(H)N) was prepared from $NiCl_2$·$6H_2O$ and (*R*)-**1a** (10 mM each, CH_3OH, rt, 18 h) and recrystallized from a 1:3 CH_3OH–Et_2O mixture (ca. 60% yield; colorless prism). As shown in **Fig. 6f–g**, the molecular structures with τ_5 values of 0.10–0.11 were nearly the same as the structure of FeCl$_2$((*R*)-H-PN(H)N) (τ_5 = 0.09).

2.4. Application to Ru-catalyzed asymmetric hydrogenation of ketones

The catalytic performance of the two *fac*-Ru complexes, *fac*-RuCl$_2$((*R*)-Ph-PN(H)N)(dmso) (**6**) and *fac*-[Ru((*R*)-H-PN(H)N)(dmso)$_3$](BF_4)$_2$ (**7**), was investigated with respect to asymmetric hydrogenation of the ketones **8** to the corresponding alcohols **9**. Four different types of ketone were selected (**8a**, non-chelatable and sterically demanding ketone; **8b**, non-chelatable aromatic ketone; **8c**, chelatable and sterically demanding ketone; **8d**, chelatable aromatic ketone), and the solvents were fixed as CH_3OH and *i*PrOH. The standard conditions were set to [**8**]$_0$ = 1 M, [**6** or **7**]$_0$ = 1 mM, [*t*BuOK]$_0$ = 10 mM, 30 °C, 100 atm H_2, and 12 h. **Table 1** summarizes the results. xxxxxxxxxxxxxxxxxxxxxxxxxxxxxxxxxxxxxxxxxxxxxxxxxxxxxxxxxxxxxxxxxxxxx

With the Ru complex **6**, **8a** was slowly hydrogenated in CH_3OH to give (*S*)-**9a** with a 98:2 *S*/*R* er. Replacement of CH_3OH with *i*PrOH attained full conversion without deterioration of the enantioselectivity (entries 1 and 2). Decreasing the amount of *t*BuOK to a three molar equivalent to Ru led to a significant decrease in reactivity (entry 3). Aromatic ketone **8b** was quantitatively hydrogenated but with lower enantioselectivity (entry 4). The complex showed little reactivity toward chelatable ketones **8c** and **8d** either in the

a CuCl((*R*)-H-PN(H)N)

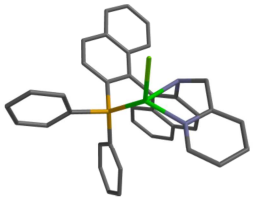

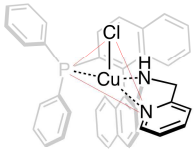

$sp^2N–Cu–sp^3P$	132.73	$sp^3N–Cu$	2.403
$sp^2N–Cu–Cl$	99.60	$sp^3P–Cu$	2.158
$sp^3P–Cu–Cl$	127.40	$sp^2N–Cu$	2.010
$sp^3N–Cu–sp^3P$	99.18	Cl–Cu	2.283
$sp^3N–Cu–sp^2N$	78.66	τ_4	0.96
$sp^3N–Cu–Cl$	95.45		

b $FeCl_2$((*R*)-H-PN(H)N)

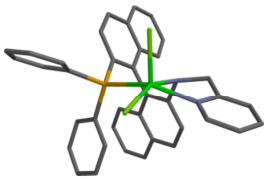

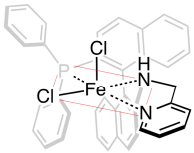

$sp^2N–Fe–sp^3N$	75.34	$sp^2N–Fe–sp^3P$	149.39
$sp^3N–Fe–sp^3P$	84.15	$sp^3N–Fe–Cl$(basal)	154.91
$sp^3P–Fe–Cl$(basal)	95.45	$sp^3N–Fe$	2.306
Cl(basal)–Fe–sp^2N	93.85	$sp^3P–Fe$	2.536
$sp^2N–Fe–Cl$(apical)	109.11	$sp^2N–Fe$	2.152
$sp^3N–Fe–Cl$(apical)	95.85	Cl(basal)–Fe	2.345
$sp^3P–Fe–Cl$(apical)	95.21	Cl(apical)–Fe	2.293
Cl(basal)–Fe–Cl(apical)	109.15	τ_5	0.09

c $FeBr_2$((*R*)-H-PN(H)N)

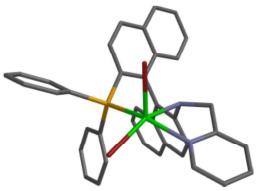

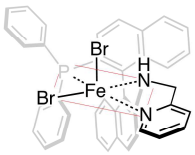

$sp^2N–Fe–sp^3N$	75.08	$sp^2N–Fe–sp^3P$	149.16
$sp^3N–Fe–sp^3P$	83.76	$sp^3N–Fe–Br$(basal)	157.71
$sp^3P–Fe–Br$(basal)	96.28	$sp^3N–Fe$	2.304
Br(basal)–Fe–sp^2N	95.12	$sp^3P–Fe$	2.556
$sp^2N–Fe–Br$(apical)	109.07	$sp^2N–Fe$	2.166
$sp^3N–Fe–Br$(apical)	94.96	Br(basal)–Fe	2.489
$sp^3P–Fe–Br$(apical)	94.69	Br(apical)–Fe	2.444
Br(basal)–Fe–Br(apical)	107.23	τ_5	0.14

d $FeCl_2$((*R*)-Ph-PN(H)N)

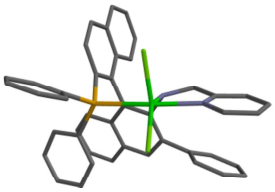

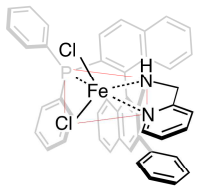

$sp^2N–Fe–sp^3N$	76.55	$sp^2N–Fe–sp^3P$	162.88
$sp^3N–Fe–sp^3P$	86.36	$sp^3N–Fe–Cl$(basal)	136.44
$sp^3P–Fe–Cl$(basal)	96.90	$sp^3N–Fe$	2.223
Cl(basal)–Fe–sp^2N	94.77	$sp^3P–Fe$	2.610
$sp^2N–Fe–Cl$(apical)	97.11	$sp^2N–Fe$	2.174
$sp^3N–Fe–Cl$(apical)	96.78	Cl(basal)–Fe	2.297
$sp^3P–Fe–Cl$(apical)	85.88	Cl(apical)–Fe	2.328
Cl(basal)–Fe–Cl(apical)	126.78	τ_5	0.43

e $FeBr_2$((*R*)-Ph-PN(H)N)

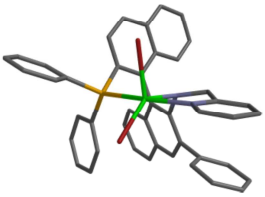

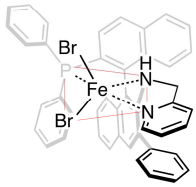

$sp^2N–Fe–sp^3N$	76.98	$sp^2N–Fe–sp^3P$	163.33
$sp^3N–Fe–sp^3P$	88.37	$sp^3N–Fe–Br$(basal)	138.26
$sp^3P–Fe–Br$(basal)	97.69	$sp^3N–Fe$	2.205
Br(basal)–Fe–sp^2N	94.20	$sp^3P–Fe$	2.631
$sp^2N–Fe–Br$(apical)	97.01	$sp^2N–Fe$	2.167
$sp^3N–Fe–Br$(apical)	97.89	Br(basal)–Fe	2.439
$sp^3P–Fe–Br$(apical)	86.04	Br(apical)–Fe	2.471
Br(basal)–Fe–Br(apical)	123.80	τ_5	0.42

f $CoCl_2$((*R*)-H-PN(H)N)

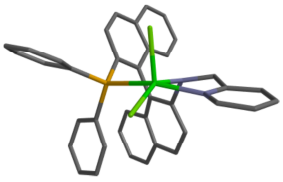

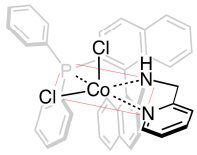

$sp^2N–Co–sp^3N$	75.35	$sp^2N–Co–sp^3P$	158.12
$sp^3N–Co–sp^3P$	86.84	$sp^3N–Co–Cl$(basal)	151.55
$sp^3P–Co–Cl$(basal)	97.21	$sp^3N–Co$	2.189
Cl(basal)–Co–sp^2N	92.78	$sp^3P–Co$	2.554
$sp^2N–Co–Cl$(apical)	103.01	$sp^2N–Co$	2.130
$sp^3N–Co–Cl$(apical)	96.86	Cl(basal)–Co	2.294
$sp^3P–Co–Cl$(apical)	91.49	Cl(apical)–Co	2.281
Cl(basal)–Co–Cl(apical)	111.10	τ_5	0.11

g $NiCl_2$((*R*)-H-PN(H)N)

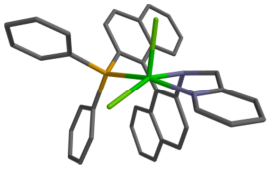

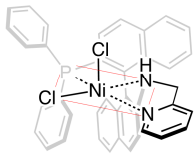

$sp^2N–Ni–sp^3N$	80.75	$sp^2N–Ni–sp^3P$	163.85
$sp^3N–Ni–sp^3P$	91.45	$sp^3N–Ni–Cl$(basal)	157.49
$sp^3P–Ni–Cl$(basal)	87.98	$sp^3N–Ni$	2.154
Cl(basal)–Ni–sp^2N	93.84	$sp^3P–Ni$	2.411
$sp^2N–Ni–Cl$(apical)	93.59	$sp^2N–Ni$	2.093
$sp^3N–Ni–Cl$(apical)	90.59	Cl(basal)–Ni	2.324
$sp^3P–Ni–Cl$(apical)	100.66	Cl(apical)–Ni	2.315
Cl(basal)–Ni–Cl(apical)	111.63	τ_5	0.10

Fig. 6. Molecular structures of the first-row transition metal complexes with (*R*)-R-PN(H)N. (a) CuCl((*R*)-H-PN(H)N). $P2_12_12_1$ (#19), a = 9.7661(11) Å, b = 9.9591(11) Å, c = 31.522(4) Å, V = 3065.9(6) Å^3, Z = 4, R = 0.0730, R_w = 0.1607. (b) $FeCl_2$((*R*)-H-PN(H)N). $P2_1$ (#4), a = 8.606(3) Å, b = 18.480(5) Å, c = 10.725(3) Å, β = 97.145(5)°, V = 1692.5(8) Å^3, Z = 2, R = 0.0411, R_w = 0.1066. (c) $FeBr_2$((*R*)-H-PN(H)N). $P2_1$ (#4), a = 8.695(3) Å, b = 18.598(6) Å, c = 10.894(4) Å, β = 98.968(4)°, V = 1740.1(9) Å^3, Z = 2, R = 0.0626, R_w = 0.1667. (d) $FeCl_2$((*R*)-Ph-PN(H)N). $P2_1$ (#4), a = 9.0539(13) Å, b = 13.605(2) Å, c = 15.771(3) Å, β = 104.378(2)°, V = 1881.8(5) Å^3, Z = 2, R = 0.0514, R_w = 0.1342. (e) $FeBr_2$((*R*)-Ph-PN(H)N). $P2_1$ (#4), a = 9.141(4) Å, b = 13.688(5) Å, c = 15.888(6) Å, β = 103.625(4)°, V = 1932.0(12) Å^3, Z = 2, R = 0.0899, R_w = 0.2566. (f) $CoCl_2$((*R*)-H-PN(H)N). P1 (#1), a = 19.747(8) Å, b = 8.725(4) Å, c = 21.648(8) Å, β = 97.563(7)°, V = 3698(3) Å^3, Z = 4, R = 0.2419, R_w = 0.6189. (g) $NiCl_2$((*R*)-H-PN(H)N). P1 (#1), a = 8.527(7) Å, b = 18.53(2) Å, c = 10.809(9) Å, β = 89.604(11)°, V = 1708(3) Å^3, Z = 2, R = 0.1972, R_w = 0.5225. τ_4 = [Σ(basal–M–basal) – Σ(basal–M–axial)]/90°. τ_5 = (α – β)/60° (α, β = basal–M–basal angles). The thin red lines in the chemical structures indicate the basal parts used for calculation of the τ values.

absence of DMSO or in the presence of 1400 mM DMSO (entries 5–8).

The performance of complex **7** was weaker than that of **6** in *i*PrOH. The sterically demanding simple ketone **8a** was hydrogenated to give, after 12 h, (*S*)-**9a** with an 87:13 er in 96% yield (entry 11). The conversion was only 10% after 2 h. In CH_3OH, however, the catalytic performance improved markedly to realize quantitative conversion and high enantioselectivity (entry 9). The reaction was completed within 2 h. The molar equivalent of *t*BuOK could be reduced to three (entry 10). In addition, aromatic ketone **8b** was hydrogenated with low enantioselectivity by complex **7** (entry 12). With the chelatable substrate **8c**, both the reactivity and enantioselectivity were low under the standard conditions (entry 13), but addition of DMSO (1400 mM) led to quantitative generation of (*S*)-**9c** with a 99:1 er (entry 14).[14b] In CH_3OH–DMSO solvent, the corresponding aromatic ketone **8d** was slowly hydrogenated to give (*R*)-**9d** with an *S*/*R* er of 10:90 (entry 15). Thus, the tertiary alkyl group is the least requirement to attain high enantioselectivity in the presentaRu-catalyzedahydrogenation.

Although there is no proof at the present stage, we think that the Ru dihydride **10** is involved in the hydrogenation (**Fig. 7**). A DACat reaction site, $H^{\delta-}$–$Ru^{\delta+}$---$N^{\delta-}$–$H^{\delta+}$, is constructed by the proton on the sp^3N ligating atom and the hydride trans to the sp^3P ligating atom. The hydride trans to the sp^2N atom is a spectator ligand. The acidic NH proton captures a ketonic substrate via a hydrogen bond with the C=O oxygen atom to move to the transition states $\mathbf{TS_S}$ and $\mathbf{TS_R}$, in which $\mathbf{TS_R}$ suffers from steric repulsion between the CH_3 group of a coordinating DMSO trans to sp^3N and the *tert*-alkyl substituent on C=O, leading to the *S* product (R^2 < *t*Bu) via $\mathbf{TS_S}$. A synergistic electrostatic and orbital effect of the electron donative sp^3N atom strengthens the Ru---S=O bond, and the degree is further enhanced by the formation of a hydrogen bond between the hydrogen atom at C(6) of the Py moiety and the oxygen atom of the DMSO. The PyC(6)H---O=S hydrogen bond fixes the DMSO conformation, creating a CH_3-fence/Py-plane chiral context. With a chelatable substrate, however, the stability of the sp^3N---Ru---S=O system is overcome, resulting in deconstruction of the chirally well-defined reactive species. This would explain why an excess amount of DMSO is required to attain high reactivity and enantioselectivity. The reason for the lack of reactivity of **6** toward a chelatable substrate even in the presence of excess DMSO is unclear. A steric effect of the C(3)Ph group might be involved. The reaction pathway from $\mathbf{TS_S}$ to **10** is controversial. According to the mechanisms proposed in the hydrogenation of acetophenone using a BINAP–Ru/diamine catalyst,[32–34] the possible pathways can be categorized into three via species **11**–**13** as shown in **Fig. 7**: i) the two hydrogen atoms in $\mathbf{TS_S}$ are simultaneously transferred to the C=O group to generate *fac*-RuH((*R*)-R-PNN)(dmso) (**11**) with liberation of the alcoholic product, and then the Ru amide bond of **11** is cleaved by H_2 to revive **10**; ii) the Ru hydride transfers to the C=O carbon to generate the alkoxide **12**, which is then cleaved by the H_2 molecule via **13** to liberate the product with concomitant regeneration of **10**; iii) the hydride transfer generates a coordinately unsaturated 16e Ru cation/alkoxide anion species, to which an H_2 molecule coordinates in a η^2 manner to give **13**. The alkoxide anion is quickly protonated by

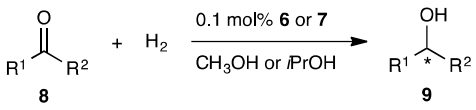

a: $R^1 = (CH_3)_3C$, $R^2 = CH_3$
b: $R^1 = C_6H_5$, $R^2 = CH_3$
c: $R^1 = (CH_3)_3C$, $R^2 = CH_2COOCH_3$
d: $R^1 = C_6H_5$, $R^2 = CH_2COOCH_3$

Table 1.
Asymmetric hydrogenation of non-chelatable and chelatable ketones using *fac*-$RuCl_2$((*R*)-Ph-PN(H)N)(dmso) (**6**) and *fac*-[Ru((*R*)-H-PN(H)N)(dmso)$_3$]$(BF_4)_2$ (**7**)[a]

Entry	Ru complex	Substrate	*t*BuOK, mM	DMSO, mM	Solvent	% Conversion[b,c]	*S*:*R*[d]
1	**6**	**8a**	10	0	CH_3OH	19	98:2
2		**8a**	10	0	*i*PrOH	>99 (10)	98:2
3		**8a**	3	0	*i*PrOH	<1	—
4		**8b**	10	0	*i*PrOH	>99 (10)	86:14
5		**8c**	10	0	*i*PrOH	<1	—
6		**8c**	10	1400	*i*PrOH	<1	—
7		**8d**	10	0	*i*PrOH	<1	—
8		**8d**	10	1400	*i*PrOH	<1	—
9	**7**	**8a**	10	0	CH_3OH	>99 (>99)	98:2
10		**8a**	3	0	CH_3OH	>99	98:2
11		**8a**	10	0	*i*PrOH	96 (10)	87:13
12		**8b**	10	0	CH_3OH	>99	37:63
13		**8c**	10	0	CH_3OH	22	85:15
14		**8c**	10	1400	CH_3OH	>99[e]	99:1
15		**8d**	10	1400	CH_3OH	32	10:90

[a]Conditions: [**8**]$_0$ = 1 M; [**6** or **7**]$_0$ = 1 mM; 30 °C; 100 atm H_2; 12 h.

[b]The ^{1}H-NMR analysis indicates that the conversion is quantitative to the yield of **9**.

[c]Values in parentheses are the results after 2 h.

[d]Determined by GC or HPLC analysis.

[e]24 h.

the highly acidic hydrogen atom on the η^2-coordinating H_2 molecule to give the alcohol product and **10**. A theoretical calculation present by Gordon and colleagues strongly supports pathway iii.[35] The reaction pathways via **11**, **12**, and **13** would be subtly affected by solvent. For example, differences in polarity, dielectric constant, and acidity between CH_3OH and *i*PrOH may change the pathway. The observed reverse solvent effect depending on the presence or absence of the C(3)Ph substituent would be related both to the preliminary step (k_0^6 and k_0^7) toward **10** from **6** and **7**, and to the catalytic cycle itself via **11**, **12**, or **13** with the rate constant k_1^6 for **6** and k_1^7 for **7**. The dicationic Ru complex **7**, which has high oxidizing power, would be easily reduced even by CH_3OH with its poor reducing ability, whereas the neutral $RuCl_2$ complex **6** would require *i*PrOH with stronger reducing ability to generate the RuH_2 species **10**. A steric effect of the C(3)Ph substituent and *i*PrOH may also exert a subtle effect on product generation. In the case of both the C(3)-Ph substituted **6** and the C(3)-non-substituted **7**, the turnover efficiency of the RuH_2 species **10** is thought to not differ significantly. The higher acidity and the smaller size of CH_3OH in comparison to *i*PrOH would facilitate generation of the intermediaries **11**, **12**, and **13** and stabilize these species via a hydrogen bond network, leading to the higher reactivity observed in CH_3OH. The rate relationships, $k_0^7 > k_0^6$ and $k_1^7 \approx k_1^6$, are thought to be responsible for the reverse solvent effect. In addition, as compared with CH_3OK, the more basic *i*PrOK would increase the contribution of the potassium amidate species, *fac*-RuH_2((*R*)-R-PN(K)N)(dmso), which has a different reactivity from *fac*-RuH_2((*R*)-R-PN(H)N)(dmso) (**10**) itself, thereby

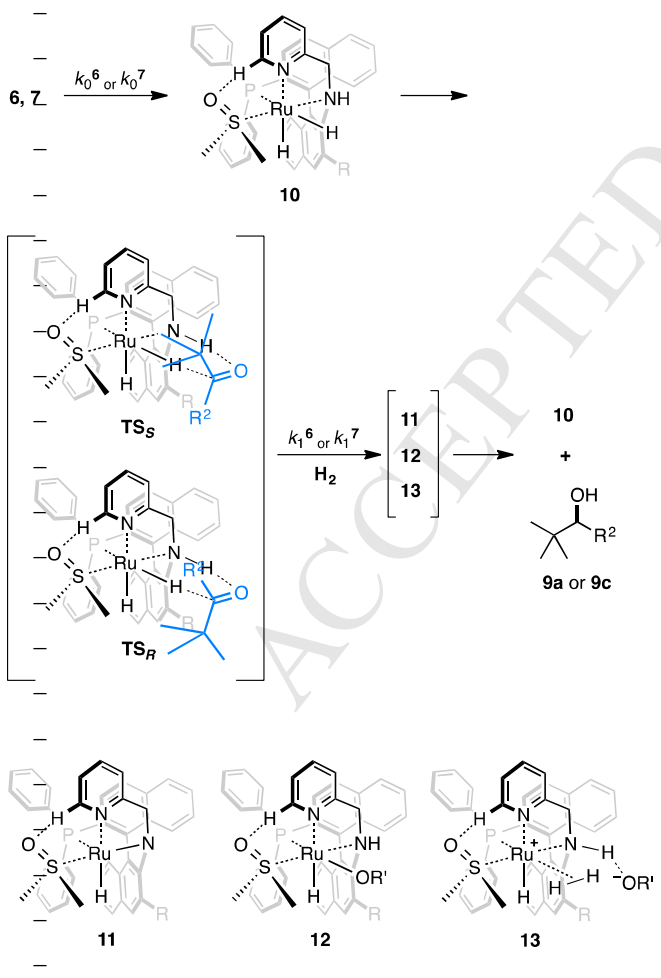

Fig. 7. Supposed reactive species and reaction pathways. R' = CH_3, $CH(CH_3)_2$, or $C(R^2)t$Bu. R^2 = CH_3 or CH_2COOCH_3.

changing the overall rate.[35,36] A more detailed mechanistic study is required for complete understanding of the present asymmetric hydrogenation.

3. Conclusion

A new chiral tridentate $sp^3P/sp^3NH/sp^2N$-combined ligand, R-PN(H)N (**1**), has been developed as an extension of sp^3P/sp^3P bidentate BINAP chemistry. The tridentate property provides an advantage over bidentate ligands by suppressing ligand dissociation or disproportionation to a 2:1 ligand/metal complex; by contrast, a serious disadvantage is associated with the linear and flexible **1** is *fac*/*mer* selectivity in terms of the formation of octahedral transition metal complexes, which constitutes an essential component of asymmetric molecular catalysis. This problem of ambiguous geometry has been overcome, by using both Gauche-type steric repulsion in the ligand and the DMSO effect that trans coordination of DMSO-*S* is energetically disfavored, to realize the selective synthesis of *fac*-$RuCl_2$((*R*)-Ph-PN(H)N)(dmso) (**6**) and *fac*-[Ru((*R*)-H-PN(H)N)$(dmso)_3$]$(BF_4)_2$ (**7**). The three different facially arranged ligating atoms—namely, the soft sp^3P, hard and highly σ-donative sp^3N, and in-between sp^2N—in R-PN(H)N electronically exert a significantly different effect on the trans coordination sites, weakening the Ru–DMSO bond trans to sp^3P and strengthening the Ru–DMSO bond trans to sp^3N. Furthermore, the conformation of the sp^3N-trans DMSO is fixed by a PyC(6)H---O=S hydrogen bond that not only makes the Ru–DMSO bond strong but also constructs a clear DMSO-CH_3-fence/Py-plane chiral context. The presence of the single sp^3NH function in the ligand simplifies the construction of an Intramol-DACat reaction site, H–Ru---sp^3N–H, in which the RuH will be generated at the most labile coordination site trans to sp^3P. These steric and electronic factors can be synergistically altered to attain the efficient hydrogenation of sterically demanding ketones with high enantioselectivity. aaaaaaaaaaaaaaaaaaa

In addition, a series of first-row transition metal (Cu(I), Fe(II), Co(II), and Ni(II)) complexes of H-PN(H)N (**1a**) and Ph-PN(H)N (**1b**) were prepared, and their non-octahedral geometries were analyzed in detail. In particular, the characteristics of the $sp^3P/sp^3NH/sp^2N$-combined ligand have realized the first synthesis of a TMP Cu(I) complex with τ_4 = 0.96, and the presence or absence of the C(3)-Ph substituent changes the SMP and TBP geometries. We hope that the present study will stimulate our ideas for the development of further chiral ligands.

Acknowledgments

This work was aided by a Grant-in-Aid for Scientific Research (No. 25E07B212) and (23005914) from the Ministry of Education, Culture, Sports, Science and Technology (Japan), and an Advanced Catalytic Transformation Program for Carbon Utilization (ACT-C) from Japan Science and Technology Agency (JST).

References and notes

1. (a) Yoshimura, M.; Tanaka, S.; Kitamura, M. *Tetrahedron Lett.* **2014**, *55*, 3635; (b) Ohkuma, T.; Kitamura, M.; Noyori, R. "*New Frontiers in Asymmetric Catalysis*" Eds. by Mikami, K.; Lautens, M. John Wiley Sons, Weinheim, 2007, pp 1–32; (c) Noyori, R.; Kitamura, M.; Ohkuma, T. *Proc. Natl. Acad. Sci.* **2004**, *101*, 5356.
2. Yoon, T. P.; Jacobsen, E. N. *Science* **2003**, *299*, 1691.
3. For example, Li: (a) Nishimura, K.; Tomioka, K. *Yakugaku Zasshi* **2003**, *123*, 9; (b) Iguchi, M.; Tomioka, K. *Org. Lett.* **2002**, *4*, 4329; Zn: (c) Oppolzer, W.; Radinov, R. N. *Tetrahedron Lett.* **1988**, *29*, 5645; Cu: (d) Zhang, D.-Y.; Shao, L.; Xu, J.; Hu, X.-P. *ACS Catal.* **2015**, *5*, 5026; (e) Duncan, A. P.; Leighton, J. L. *Org.*

Lett. **2004**, *6*, 4117; Pd: (f) Sakaguchi, S.; Yoo, K. S.; O'Neill, J.; Lee, J. H.; Stewart, T.; Jung, K. W. *Angew. Chem. Int. Ed.* **2008**, *47*, 9326.

4. Chiral arene: (a) Therrien, B.; Süss-Fink, G. *Inorg. Chim. Acta* **2004**, *357*, 219; (b) Pape, A. R.; Kaliappan, K. P.; Kündig, E. P. *Chem. Rev.* **2000**, *100*, 2917; (c) Bolm, C.; Muñiz, K. *Chem. Soc. Rev*. **1999**, *28*, 51; chiral Cp: (d) Kossler, D.; Cramer, N. *J. Am. Chem. Soc*. **2015**, *137*, 12478; (e) Ye, B.; Cramer, N. *Science* **2012**, *338*, 504; (f) Siemeling, U. *Chem. Rev.* **2000**, *100*, 1495; (g) Halterman, R. L. *Chem. Rev*. **1992**, *92*, 965.
5. Reviews and book: (a) Riordan, C. G. *Coord. Chem. Rev.* **2010**, *254*, 1815; (b) Rapenne, G. *Inorg. Chim. Acta* **2009**, *362*, 4276; (c) Scorpionates II: Chelating Borate Ligands; Pettinari, C., Ed.; Imperiall College Press: London, UK, 2008; (d) Gibson, S. E.; Castaldi, M. P. *Chem. Commun.* **2006**, 3045; some examples: (e) Kitamura, M.; Takenaka, Y.; Okuno, T.; Holl, R.; Wünsch, B. *Eur. J. Inorg. Chem*. **2008**, 1188; (f) Foltz, C.; Enders, M.; Bellemin-Laponnaz, S.; Wadepohl, H.; Gade, L. H. *Chem. Eur. J*. **2007**, *13*, 5994; (g) Dro, C.; Bellemin-Laponnaz, S.; Welter, R.; Gade, L. H. *Angew. Chem. Int. Ed.* **2004**, *43*, 4479; (h) Zhou, J.; Ye, M.-C.; Tang, Y. *J. Comb. Chem.* **2004**, *6*, 301; (i) Keyes, M. C.; Chamberlain, B. M.; Caltagirone, S. A.; Halfen, J. A.; Tolman, W. B. *Organometallics* **1998**, *17*, 1984; (j) Burk, M. J.; Harlow, R. L. *Angew. Chem. Int. Ed. Engl.* **1990**, *29*, 1462.
6. NNN: (a) Talsi, E. P.; Bryliakov, K. P. *Coord. Chem. Rev.* **2012**, *256*, 1418; (b) Nonoyama, M.; Sakai, K. *Inorg. Chim. Acta* **1983**, *72*, 57; OOO: (c) Curtis, W. D.; Laidler, D. A.; Stoddart, J. F.; Jones, G. H. *J. Chem. Soc. Chem. Commun*. **1975**, 833; SSS: (d) Forsyth, G. A.; Lockhart, J. C. *J. Chem. Soc. Dalton Trans.* **1994**, 2243; PPP/PNN: (e) Edwards, P. G.; Kariuki, B. M.; Newman, P. D.; Tallis, H. A.; Williams, C. *Dalton Trans.* **2014**, *43*, 15532.
7. Reviews: (a) Asay, M.; Morales-Morales, D. *Dalton Trans.* **2015**, *44*, 17432; (b) Deng, Q.-H.; Melen, R. L.; Gade, L. H. *Acc. Chem. Rev*. **2014**, *47*, 3162; (c) Nishiyama, H.; Itoh, J. *The Chemical Record* **2007**, *7*, 159.
8. Reviews: (a) Zhang, D.-Y.; Hu, X.-P. *Tetrahedron Lett.* **2015**, *56*, 283; (b) Pradeep, C. P.; Das, S. K. *Coord. Chem. Rev.* **2013**, *257*, 1699; some examples: (c) Tanaka, T.; Sano, Y.; Hayashi, M. *Chem. Asian J*. **2008**, *3*, 1465; (d) Gao, Y.-G.; Chen, N.; Wu, H.-J.; Li, X.-S. *Russ. J. Org. Chem.* **2007**, *43*, 1754; (e) Murtagh, K.; Sweetman, B. A.; Guiry, P. J. *Pure Appl. Chem*. **2006**, *78*, 311; (f) Hayashi, M.; Miyamoto, Y.; Inoue, T.; Oguni, N. *J. Chem. Soc. Chem. Commun.* **1991**, 1752; for a related ligand: (g) Naganawa, Y.; Namba, T.; Aoyama, T.; Shoji, K.: Nishiyama, H. *Chem. Commun*. **2014**, *50*, 13224.
9. (a) Clarke, M. L. *Synlett* **2014**, *25*, 1371; (b) Darwish, M. O.; Wallace, A.; Clarkson, G. J.; Wills, M. *Tetrahedron Lett*. **2013**, *54*, 4250; (c) Xie, J.-H.; Liu, X.-Y.; Xie, J.-B.; Wang, L.-X.; Zhou, Q.-L. *Angew. Chem. Int. Ed*. **2011**, *50*, 7329; (d) Lee, J.-Y.; Miller, J. J.; Hamilton, S. S.; Sigman, M. S. *Org. Lett*. **2005**, *7*, 1837.
10. R = H: H-PN(H)N (2'-(diphenylphosphanyl)-*N*-(pyridin-2-ylmethyl)- [1,1'-binaphthalen]-2-amine); R = C_6H_5: Ph-PN(H)N (2'-(diphenylphosphanyl)-3-phenyl-*N*-(pyridin-2-ylmethyl)-[1,1'-binaphthalen]-2-amine).
11. (a) Kitamura, M.; Nakatsuka, H. *Chem. Commun*. **2011**, *47*, 842; (b) Noyori, R. *Angew. Chem. Int. Ed.* **2002**, *41*, 2008.
12. Nishiyama, H.; Sakaguchi, H.; Nakamura, T.; Horihata, M.; Kondo, M.; Itoh, K. *Organometallics* **1989**, *8*, 846.
13. The original reaction for deducing an intramolecular metathesis-type DACat concept (Intramol-MDACat): (a) Noyori, R.; Kitamura, M. *Angew. Chem. Int. Ed*. **1991**, *30*, 49; (b) Kitamura, M.; Okada, S.; Suga, S.; Noyori, R. *J. Am. Chem. Soc*. **1989**, *111*, 4028; (c) Kitamura, M.; Suga, S.; Kawai, K.; Noyori, R. *J. Am. Chem. Soc*. **1986**, *108*, 6071; for intermolecular metathesis-type DACat (Intermol-MDACat): (d) Kitamura, M.; Ohkuma, T.; Inoue, S.; Sayo, N.; Kumobayashi, H.; Akutagawa, S.; Ohta, T.; Takaya, H.; Noyori, R. *J. Am. Chem. Soc*. **1988**, *110*, 629; (e) Noyori, R.; Ohkuma, T.; Kitamura, M.; Takaya, H.; Sayo, N.; Kumobayashi, H.; Akutagawa, S. *J. Am. Chem. Soc*. **1987**, *109*, 5856; Intramol-redox-involved DACat (Intramol-RDACat): (f) Tanaka, S.; Suzuki, Y.; Saburi, H.; Kitamura, M. *Tetrahedron* **2015**, *71*, 6559; (g) Saburi, H.; Tanaka, S.; Kitamura, M. *Angew. Chem. Int. Ed*. **2005**, *44*, 1730; (h) Tanaka, S.; Saburi, H.; Ishibashi, Y.; Kitamura, M. *Org. Lett*. **2004**, *6*, 1873; Intramol-RDACat: (i) Miyata, K.; Kutsuna, H.; Kawakami, S.; Kitamura, M. *Angew. Chem. Int. Ed.* **2011**, *50*, 4649; see also: (j) Kitamura, M.; Tanaka, S.; Yoshimura, M. *J. Synth. Org. Chem. Jpn.* **2015**, *137*, 690; (k) Kitamura, M.; Miyata, K.; Seki, T.; Vatmurge, N.; Tanaka, S. *Pure Appl. Chem.* **2013**, *85*, 1121; (l) Miyata, K.; Kitamura, M. *Synthesis* **2012**, *44*, 2138.
14. (a) Nakatsuka, H.; Yamamura, T.; Shuto, Y.; Tanaka, S.; Yoshimura, M.; Kitamura, M. *J. Am. Chem. Soc*. **2015**, *137*, 8138; (b) Yamamura, T.; Nakatsuka, H.; Tanaka, S.; Kitamura, M. *Angew. Chem. Int. Ed*. **2013**, *52*, 9313; (c) Huang, H.; Okuno, T.; Tsuda, K.; Yoshimura, M.; Kitamura, M. *J. Am. Chem. Soc*. **2006**, *128*, 8716.
15. (a) Ohkuma, T.; Sandoval, C. A.; Srinivasan, R.; Lin, Q.; Wei, Y.; Muñiz, K.; Noyori, R. *J. Am. Chem. Soc*. **2005**, *127*, 8288; (b) Noyori, R.; Ohkuma, T. *Angew. Chem. Int. Ed*. **2001**, *40*, 40; (c) Ohkuma, T.; Ooka, H.; Hashiguchi, S.; Ikariya, T.; Noyori, R. *J. Am. Chem. Soc*. **1995**, *117*, 2675.
16. Bifunctional Molecular Catalysis; Ikariya, T., Shibasaki, M., Eds.; Springer: Heidelberg, Germany, 2011.
17. sp^3NH_2/sp^3NH_2: ref 15c; (a) Guo, R.; Lough, A. J.; Morris, R. H.; Song, D. *Organometallics* **2004**, *23*, 5524; sp^3NH_2/sp^3NH: (b) Clarke, M. L.; Díaz-Valenzuela, M. B.; Slawin, A. M. Z. *Organometallics* **2007**, *26*, 16; sp^3NH_2: ref 15a; (c) Dahlenburg, L.; Kühnlein, C. *J. Organomet. Chem.* **2005**, *690*, 1; sp^3NH/sp^3NH: ref 14a; (d) Gao, J.-X.; Ikariya, T.; Noyori, R. *Organometallics* **1996**, *15*, 1087.
18. Ishibashi, Y.; Bessho, Y.; Yoshimura, M.; Tsukamoto, M.; Kitamura, M. *Angew. Chem. Int. Ed*. **2005**, *44*, 7287.
19. Shi, M.; Chen, L.-H.; Li, C.-Q. *J. Am. Chem. Soc*. **2005**, *127*, 3790.
20. See supprementary material.
21. Botman, P. N.; David, O.; Amore, A.; Dinkelaar, J.; Vlaar, M. T.; Goubitz, K.; Fraanje, J.; Schenk, H.; Hiemstra, H.; Maarseveen, J. H. *Angew. Chem. Int. Ed*. **2004**, *43*, 3471.
22. For the geometry abbreviation, see: Nomenclature of Inorganic Chemistry, IUPAC Recommendations 2005 (Red Book I), old.iupac.org—Red_Book_2005.pdf
23. Artero, V.; Laurencin, D.; Villanneau, R.; Thouvenot, R.; Herson, P.; Gouzerh, P.; Proust, A. *Inorg. Chem*. **2005**, *44*, 2826.
24. Reviews: (a) Calligaris, M. *Coord. Chem. Rev*. **2004**, *248*, 351; (b) Alessio, E. *Chem. Rev*. **2004**, *104*, 4203.
25. Zeng, F.; Yu, Z. *Organometallics* **2009**, *28*, 1855.
26. Toyama, M.; Iwamatsu, S.; Inoue, K.; Nagao, N. *Bull. Chem. Soc. Jpn*. **2010**, *83*, 1518.
27. Supporting information in ref 14b.
28. τ_4: (a) Addison, A. W.; Rao, T. N. *J. Chem. Soc. Dalton Trans.* **1984**, 1349; τ_5: Vela, J.; Cirera, J.; Smith, J. M.; Lachicotte, R. J.; Flaschenriem, C. J.; Alvarez, S.; Holland, P. L. *Inorg. Chem.* **2007**, *46*, 60.
29. Some examples: (a) Martín, C.; Whiteoak, C. J.; Martin, E.; Escudero-Adán, E. C.; Galán-Mascarós, J. R.; Kleij, A. W. *Inorg. Chem*. **2014**, *53*, 11675; (b) Searls, C. E.; Kleespies, S. T.; Eppright, M. L.; Schwartz, S. C.; Yap, G. P. A.; Scarrow, R. C. *Inorg. Chem*. **2010**, *49*, 11261; (c) Mattews, C. J. *Annu. Rep. Prog. Chem. Sect. A* **2004**, *100*, 177; (d) Ray, M.; Hammes, B. S.; Yap, G. P. A.; Rheingold, A. L.; Borovik, A. S. *Inorg. Chem.* **1998**, *37*, 1527; (e) Mealli, C.; Ghilardi, C. A.; Orlandini, A. *Coord. Chem. Rev*. **1992**, *120*, 361.
30. Suzuki, T.; Wasada-Tsutsui, Y.; Ogawa, T.; Inomata, T.; Ozawa, T.; Sakai, Y.; Fryzuk, M. D.; Masuda, H. *Inorg. Chem*. **2015**, *54*, 9271.
31. τ_4 = 1.2: Bagchi, V.; Paraskevopoulou, P.; Das, P.; Chi, L.; Wang, Q.; Choudhury, A.; Mathieson, J. S.; Cronin, L.; Pardue, D. B.; Cundari, T. R.; Mitrikas, G.; Sanakis, Y.; Stavropoulos, P. *J. Am. Chem. Soc*. **2014**, *136*, 11362.
32. (a) Hasanayn, F.; Morris, R. H. *Inorg. Chem.* **2012**, *51*, 10808; (b) Iuliis, M. Z.-D.; Morris, R. H. *J. Am. Chem. Soc*. **2009**, *131*, 11263; (c) Hadzovic, A.; Song, D.; MacLaughlin, C. M.; Morris, R. H. *Organometallics* **2007**, *26*, 5987; (d) Abdur-Rashid, K.; Clapham, S. E.; Hadzovic, A.; Harvey, J. N.; Lough, A. J.; Morris, R. H. *J. Am. Chem. Soc.* **2002**, *124*, 15104; (e) Abdur-Rashid, K.; Faatz, M.; Lough, A. J.; Morris, R. H. *J. Am. Chem. Soc.* **2001**, *123*, 7473; *cis* RuH_2: (f) Abbel, R.; Abdur-Rashid, K.; Faatz, M.; Hadzovic, A.; Lough, A. J.; Morris, R. H. *J. Am. Chem. Soc.* **2005**, *127*, 1870; (g) Abdur-Rashid, K.; Abbel, R.; Hadzovic, A.; Lough, A. J.; Morris, R. H. *Inorg. Chem.* **2005**, *44*, 2483.
33. (a) John, J. M.; Takebayashi, S.; Dabral, N.; Miskolzie, M.; Bergens, S. H. *J. Am. Chem. Soc.* **2013**, *135*, 8578; (b) Takebayashi, S.; Dabral, N.; Miskolzie, M.; Bergens, S. H. *J. Am. Chem. Soc.* **2011**, *133*, 9666; (c) Hamilton, R. J.; Bergens, S. H. *J. Am. Chem. Soc*. **2008**, *130*, 11979; (d) Hamilton, R. J.; Bergens, S. H. *J. Am. Chem. Soc.* **2006**, *128*, 13700; (e) Hamilton, R. J.; Leong, C. G.; Bigam, G.; Miskolzie, M.; Bergens, S. H. *J. Am.*

Chem. Soc. **2005**, *127*, 4152; (f) Daley, C. J. A.; Bergens, S. H. *J. Am. Chem. Soc.* **2002**, *124*, 3680.
34. (a) Sandoval, C. A.; Ohkuma, T.; Muñiz, K.; Noyori, R. *J. Am. Chem. Soc.* **2003**, *125*, 13490; (b) Yamakawa, M.; Yamada, I.; Noyori, R. *Angew. Chem. Int. Ed.* **2001**, *40*, 2818.
35. Dub, P. A.; Henson, N. J.; Martin, R. L.; Gordon, J. C. *J. Am. Chem. Soc.* **2014**, *136*, 3505.
36. (a) Hartmann, R.; Chen, P. *Adv. Synth. Catal.* **2003**, *345*, 1353; (b) Hartmann, R.; Chen, P. *Angew. Chem. Int. Ed.* **2001**, *40*, 3581.

Supplementary Material

Supplementary data associated with this article can be found in the online version at XXXX. These data include details of experimental procedures, NMR spectroscopic data, X-ray crystallographic data (CIF) for ligands and metal complexes, and Ru-catalyzed asymmetric hydrogenation. This material is available free of charge via the Internet at XXX. The X-ray diffraction data can be obtained free of charge from the Cambridge Crystallographic Data Centre via www.ccdc.cam.ac.uk—data_re-quest/cif.